



Seismic performance of structure equipped with a new rubber bracing damper system

Farzad Hejazi¹ · Hengameh Farahpour² · Najad Ayyash²

Received: 8 June 2023 / Revised: 31 October 2023 / Accepted: 2 December 2023 / Published online: 25 January 2024
© The Author(s) 2024

Abstract

Nowadays, vibration energy absorption devices are widely implemented in many buildings subjected to severe vibration due to natural hazards, such as earthquakes, strong winds, and typhoons. Recently, viscous dampers have been commonly used in many structures as the most conventional damper type. However, the high maintenance cost resulting from oil leakage from cylinder seals has prompted researchers to seek an alternative system to viscous damper systems. Therefore, the main aim of this research is to develop a new rubber bracing damper (RBD) system by implementing high damping rubber material as a viscoelastic material to be installed in framed structures as diagonal bracing members. This will help dissipate vibration effects on the structure. To achieve this, the initial design for the RBD device has been developed, and finite-element simulation has been conducted to evaluate the behavior of the proposed RBD under various dynamic loading conditions. To define the viscoelastic material properties in finite-element modeling, high damping rubber material has been produced and experimentally tested to determine the numerical model of the material. Subsequently, the test data were utilized to develop the analytical model of the RBD device, and its performance was evaluated by applying cyclic loads and conducting nonlinear analysis. Furthermore, a series of cyclic dynamic tests with various displacement amplitudes and frequencies have been conducted on the prototype of the RBD device based on the finite-element results. Finally, to analyze the dynamic behavior of the structure equipped with RBD, a finite-element model of a three-story reinforced concrete frame structure furnished with RBD dampers has been developed. The response of the structure has been evaluated under seismic loads, and a parametric study has been conducted to investigate the response of the structures with various rubber properties. The numerical analysis results indicated that the implementation of the RBD device leads to a reduction in the occurrence of plastic hinges and lateral displacements of the structure by up to 69%. This demonstrates the efficiency of the RBD device in diminishing the seismic load effect on the structure's response.

Keywords Rubber bracing damper · Seismic · Passive control · Vibration · Viscoelastic model · Parametric study

1 Introduction

The tremendous socioeconomic effects of earthquakes cannot be completely avoided, but they can be significantly mitigated by implementing proper structural design practices. Recently, the utilization of supplementary innovative devices in both new and existing structures has been recognized as a suitable and cost-effective solution.

Several valuable published studies have demonstrated the success of these devices in reducing the forces and deformations experienced by structural elements. This is achieved by modifying the dynamic properties of the system, thereby implementing the concept of structural response control and energy dissipation through this technology.

The passive control method, as the oldest and most common structural response control technique, has been extensively studied in numerous research studies. The prevailing concept followed by most of the literature is to incorporate discrete elements, known as dampers, into the structure due to their minimal maintenance requirements and independence from power supply. These dampers are strategically installed in the framing system to connect various parts and provide additional damping to dissipate energy.

✉ Farzad Hejazi
farzad.hejazi@uwe.ac.uk

¹ Faculty of Environment and Technology, The University of the West England, Bristol, UK

² Department of Civil Engineering, Faculty of Engineering, University Putra Malaysia, Serdang, Malaysia

In rate-dependent devices, the energy dissipation function simultaneously depends on both the velocity and the displacement of the excitation. Viscous fluid (VFD), viscoelastic (VE), and viscous wall dampers are three recognized classes of this category. An integrated semi-active adaptive vibration control system, consisting of a semi-active bypass fluid damper and a programmable logic controller, has been developed to protect bridges from varying traffic loads. Through experimental tests and numerical analysis, the system's effectiveness in generating a wide range of forces and effectively limiting bridge displacements has been demonstrated [3]. A new seismic resisting technique was proposed for reinforced concrete frame buildings through combining of a rubber core and a U-shaped friction damping system. The results revealed that the maximum shear strength, stiffness, and energy dissipation capacities of structure furnished with this device were significantly improved (Rahnavard et al. [14]).

A variable stiffness pneumatic spring–oil damper was proposed to eliminate the shortcomings of traditional dampers in a high-rise steel structure. This device can significantly decrease peak displacement and inter-story drift angles [22]. In a theoretical and experimental investigation, the application of lead rubber dampers (LRD) in the chevron bracing was evaluated. The results indicated that significant reductions in the stories' drift can be achieved by installing lead rubber dampers in the chevron bracing [25].

FVDs cause column loads that are out of phase with the regular column stresses, since they are dependent on velocity alone. Conversely, VE dampers cause in-phase column stresses and, for strong earthquake loads, even high stresses independent of the building displacement. In viscoelastic (VE) dampers, sandwiched viscoelastic materials, placed between the steel plates, are in charge of damping performance.

The behavior of a natural rubber bearing system (NRBs) equipped with U-shaped dampers is investigated through combined Mooney–Rivlin and Prony models in ANSYS software. Two types of analyses, involving both static and dynamic time histories, were chosen to assess the performance of NRBs that were fitted with dampers [15]. To enhance the energy dissipation capacity of viscoelastic (VE) dampers at room temperature by utilizing a blended rubber matrix to expand the working temperature range, a range of VE material samples were prepared using blended rubber matrix, and the best formula was chosen for the production of VE dampers. The performance of VE dampers based on blended rubber matrix and single rubber matrix was then tested and compared [21]. Also, an innovative use of natural rubber pads in chevron braces as an autonomous seismic force resisting system was investigated. Results showed that this system provided additional damping and also shifted the period of structure [4].

A new type of lead-viscoelastic coupling beam damper (LVCBD) has been suggested due to the poor fatigue performance of the metallic-type RCBD and the sensitivity of the viscoelastic-type RCBD to loading frequency. The LVCBD is not affected by loading frequency and has superior fatigue performance and energy dissipation capacity [2].

A lever-based damper called the rotation-magnified viscoelastic damper (RMVD) was created to enhance the angular deformation at beam–column joints. This amplified the shear deformation and energy dissipation of viscoelastic materials, resulting in optimal energy dissipation [8].

Using a method based on probability has been suggested to calculate the remaining displacement of a trilinear hysteretic system that represents a highway bridge with unbonded laminated rubber bearings (ULRBs) and transverse steel dampers (TSDs). This approach takes into account the uncertainty of structural parameters and the variation of ground motions [23].

A new type of damper called the lead-viscoelastic coupling beam damper (LVCBD) developed to address the issues with current rotational viscoelastic dampers (RVEDs) in steel buckling-restrained braced frames (SBRBFs). The LVCBD has better fatigue performance and energy dissipation capacity and is not affected by loading frequency. It can be installed without requiring additional architectural space and can increase the inherent damping of the SBRBF by around 3% [16]. In another research, high damping rubber devices were added to the bracing of a steel frame, but tests' output did not show significant changes in stiffness and damping of structure [1].

The development of the VE dampers in different shapes, configurations, and materials also paved the way, and some novel ideas such as a hybrid configuration [13] and disc-shaped viscoelastic material covered by a cylindrical pipe [7] were numerically and experimentally examined. Ramakrishna in 2019 carried out a numerical study to compare natural rubber and 3M material benefits as a viscoelastic material in dampers [12]. The effectiveness of VE dampers considering the excitation uncertainty was evaluated and multiple response history analyses (RHA) were conducted by Xiang and Xie [20]. This analysis revealed that the temperature fluctuation notably affects the dispersion of the VED effectiveness.

A Visco-Hyperelastic Damper consists of a viscoelastic material sandwiched between two metal rings introduced and developed to perform a combination of the elastic behavior of the viscoelastic material and the plastic deformation of the steel parts. This device performed 82% to 99% energy dissipation based on the level of loading [10].

A new Rubber-Steel Core Damper (RSCD) device has been proposed to improve the seismic performance of chevron braced frames. The experimental results showed that the

proposed RSCD damper provides a ductile behavior with completely regular and stable hysteresis loops. [17].

A deformable elastoplastic metallic core comprising four arcs firmly attached tangentially to the central ring and then to the corner of a structural panel. Results showed a desirable balance between the added lateral rigidity and the provided damping [11].

The extensive review of the literature presented above underscores the significant capability of high damping rubber to dissipate vibrations. While it is broadly used in base isolation, but in the main structure often involves its combination with additional vibration damping systems to enhance dissipation. However, as mentioned before, rubber possesses a robust capacity to mitigate vibration, especially when effectively incorporated into buildings as a structural main component such as bracing members.

For this reason, the main aim of this research is to develop a new rubber bracing damper (RBD) device by implementing high damping natural rubber (HDNR) as an energy-dissipating component. To achieve this objective, numerical models of the proposed device, including finite-element and analytical models, have been developed. The numerical results have been compared and validated with experimental data obtained from laboratory tests conducted on a lab-size prototype of the RBD device. These tests involved applying cyclic loads using a dynamic actuator.

Subsequently, the RBD device was implemented in a three-story reinforced concrete frame structure under seismic loads to assess its performance in reducing the seismic response of the structure.

2 Development of rubber bracing damper (RBD)

In this research, a new rubber bracing damper device (Patent No. US11041323B2) has been developed as a supplementary structural element to be installed in structures subjected to extreme dynamic loads. As shown in Fig. 1, the RBD consists of an inner tube (labeled as 1), an outer cylinder, and a steel shaft (labeled as 2) serving as an inner piston rod, positioned in parallel alignment within the outer cylinder. The core extends through the cylinder tube without contacting its inner surface. High Damping Natural Rubber (HDNR) material (labeled as 3) is filled between the inner core and outer tube (between parts 1 and 2), and through a special curing process, it is bonded to the inner surface of the steel cylinder and the outer surface of the steel shaft. In this study, the high damping rubber is manufactured by vulcanizing the natural rubber compound and adding black carbon and other fillers to increase the stiffness and loss factor of the rubber. These filler materials also reduce the dependence of the material properties on temperature and loading frequency. The rubber

compounds used in this research were specifically formulated to have a higher loss factor.

A joint (labeled as 4) connects a front hinge joint (labeled as 5) to one end of the core shaft (labeled as 2), and another hinge joint (labeled as 7) is welded to the end of the outer cylinder tube (labeled as 1). An inner stopper (labeled as 6) connects the rear hinge joint (labeled as 7) to the other end of the inner core through a loss bolt, which is able to move during vibration and restrict the movement of the shaft in case of unpredictable excessive movements. The front and rear hinge joints (labeled as 5 and 7) allow the RBD device to be installed as a diagonal brace or within both beam–column connections at the bottom- and top-story levels, as depicted in Fig. 2a.

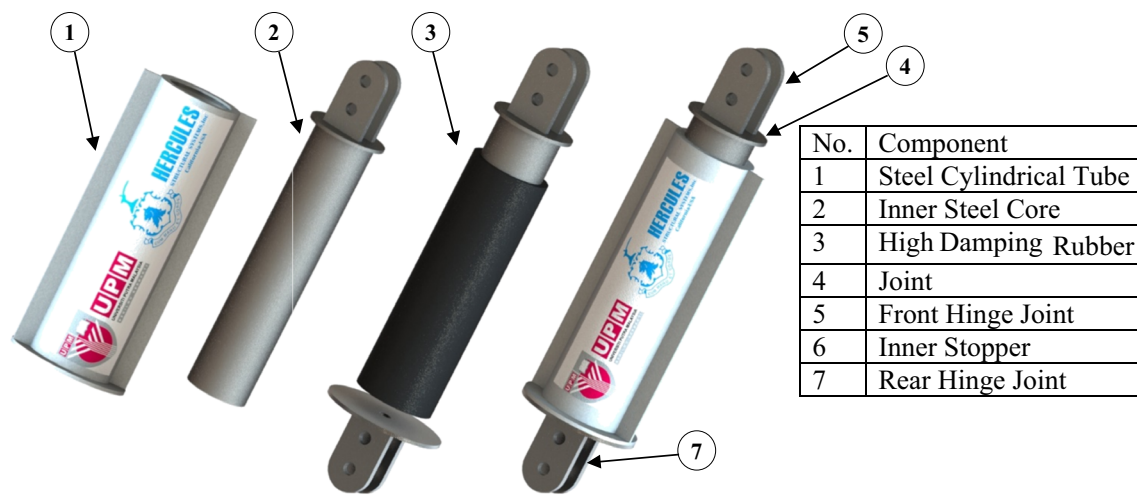
Therefore, when a lateral dynamic load is applied, the frame structure oscillates, and inter-story movements are transferred from the structure to the RBD device. As a result, the core shaft movement causes the HDNR layer (part 3), which is filled within the inner shaft and outer cylinder and bonded to their surfaces, to undergo shear deformation, as shown in Fig. 2b. The shear action of HDNR dissipates a significant portion of the excitation energy, and the remaining force is transmitted to the base of the structure through the rear hinge joint (part 7). Scientifically, this process can be explained by the force balance equation applicable to passive energy dissipation systems [19].

3 Numerical performance estimation of the RBD device

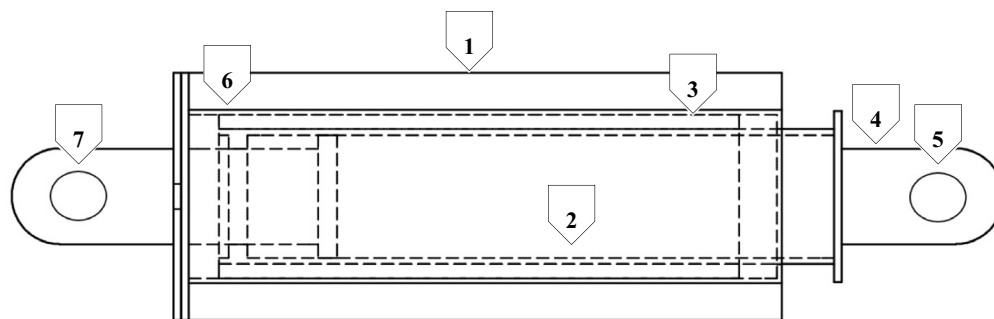
To evaluate the performance of the newly developed rubber bracing damper, a numerical model of the RBD subjected to dynamic cyclic loads is created, and the behavior of the device is investigated.

4 Development of the constitutive model for high damping natural rubber material

In this study, a special high damping natural rubber (HDNR) material with high damping capacity has been produced for use in the RBD device to achieve the desired vibration dissipation performance. Consequently, a series of experimental tests, including uniaxial and shear tests, have been conducted on casted HDNR material samples to determine the mechanical properties of the material. The strip specimens for the uniaxial test, measuring 25 mm wide by 3 mm thick and 115 mm long, are presented in Fig. 3a. The uniaxial test equipment and the deformed rubber specimen are illustrated in Fig. 3b. The specification of the rubber strip also has been reported in Table 1.



(a) Exploded and assembling views



(b) Detailed Drawing

Fig. 1 RBD configuration

To assess the shear characteristics of the manufactured rubber, shear experimental tests have been performed using cylindrical specimens with a diameter of 25 mm and a height of 6 mm. This rubber sample is shown in Fig. 4a. The shear test equipment and the rubber sample before and after applying shear force are depicted in Fig. 4b. Additionally, the deformed and torn rubber, as well as the delamination damage, can be observed in Fig. 4c.

From the uniaxial and shear experimental tests, the stress–strain relation (the constitutive model) has been extracted and illustrated in Fig. 5a and b. The results showed that the HDNR as viscoelastic material has the ability to deform elastically through large strains.

For each graph, a regression equation (fitting curve) has been derived, representing the mathematical expression of the stress–strain relation for the rubber in axial or shear loading conditions. These regression equations are highly implemented in structural nonlinear analysis as many finite-element programs and software packages use

the stress–strain formulation to define material behavior under various conditions, such as axial or shear loading.

Using third-degree polynomial fitting curves for both uniaxial and shear stress–strain graphs has resulted in a coefficient of determination (R-squared) of more than 99% for both graphs, indicating excellent reliability and accuracy of the trend curves based on the given data.

Additionally, regression reports for both axial and shear stress–strain graphs for the rubber material have been generated and included in the manuscript as Tables 2 and 3, respectively.

The uncertainty parameter for developing the constitutive model (stress–strain relation) for the rubber material using experimental test results is primarily related to the rubber composite, as high damping rubber is a product of mixing several raw materials. Therefore, in this research, the same composition for the tested high damping material in axial and shear has been used to fabricate the RBD device.

Fig. 2 Function of RBD device

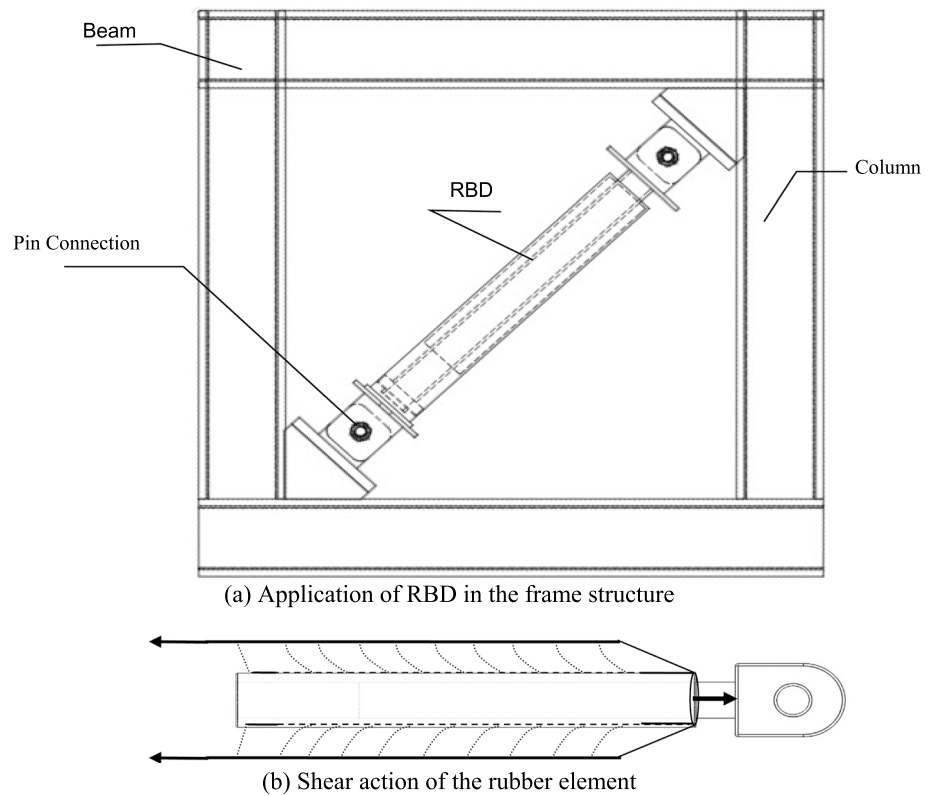


Fig. 3 Uniaxial experimental test

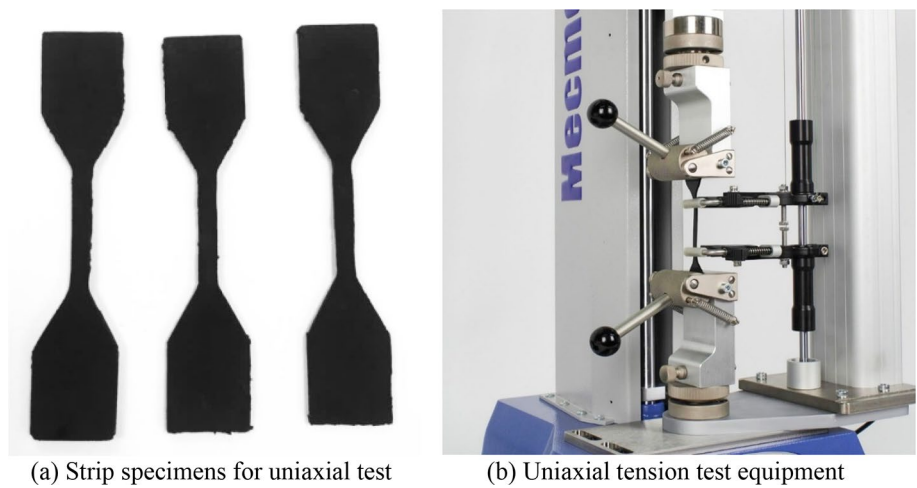


Table 1 High damping rubber specimen parameters

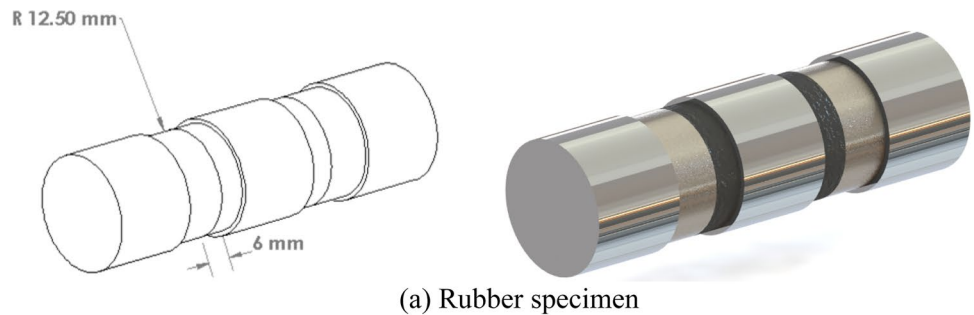
Shear modulus (MPa)	Density (kg/m ³)	Young's Modulus (MPa)	Length (mm)	Width (mm)	Thickness (mm)
1.2	1200	3.6	115	25	3

As previously mentioned, considering the complexity of the nonlinear behavior of the rubber, the material properties extracted from the experimental tests have been used

to develop the finite-element model of the HDNR layer. For this purpose, the viscoelastic stress–strain function was obtained from Eq. (1)

$$\sigma_{ij} = \frac{\partial U(\epsilon)}{\partial \epsilon_{ij}}, \tag{1}$$

where the stored strain energy function, $U(\epsilon)$, defines the strain energy stored in a material per unit volume. And σ_{ij} and ϵ_{ij} are the stress and strain components, respectively. To predict the nonlinear stress–strain curve of the material

Fig. 4 Shear experimental test details

(a) Rubber specimen



(b) Shear test equipment



(c) Deformed and teared rubber specimen

the Neo-Hookean material model has been considered with the strain energy as a function of the strain tensor invariant I_1 in Eq. (2)

$$W = \frac{\mu}{2} (\bar{I}_1 - 3) + \frac{1}{D_1} (J - 1)^2, \quad (2)$$

where μ is the initial shear modulus and D_1 is the material's incompressible parameter. If the material is assumed to be incompressible, $J = 1$, and the second term becomes

zero. Since the Neo-Hookean model works with a constant shear module, a constant shear modulus of 1.2 MPa has been added to the model and the viscoelasticity of the material modeled through Viscoelastic Shear Data and Prony Shear Relaxation [24]. The combination of these models changes the Elastic moduli according to shear modulus variations.

Viscoelastic behavior includes a viscous (time-dependent) component acting upon the elastic (time-independent) component. To model the viscous time-dependent component through the Prony series [5], the normalized shear

Fig. 5 HDNR measured experimental data

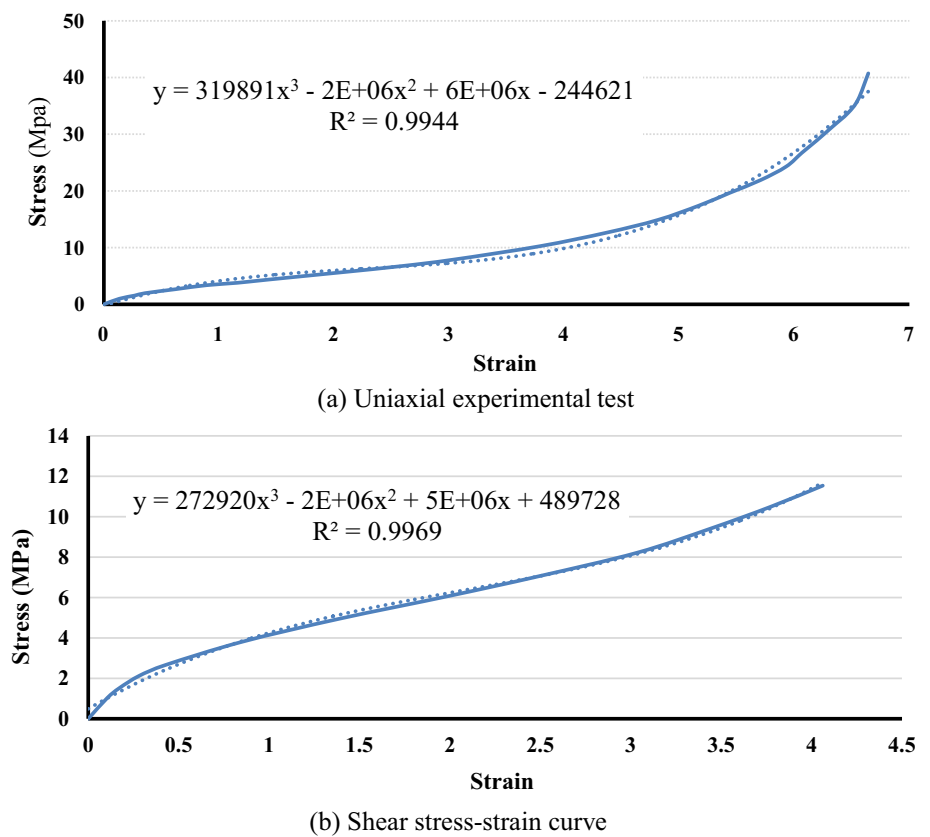


Table 2 Regression summary output for results of uniaxial experimental test of the rubber

Regression statistics								
Multiple R							0.940135	
R square							0.883853	
Adjusted R square							0.878574	
Standard error							4,449,087	
Observations							24	
ANOVA								
	<i>df</i>	SS	MS	<i>F</i>	Significance <i>F</i>			
Regression	1	3.31E+15	3.31E+15	167.4152	9.23E-12			
Residual	22	4.35E+14	1.98E+13					
Total	23	3.75E+15						
	Coefficients	Standard error	<i>t</i> Stat	<i>p</i> value	Lower 95%	Upper 95%	Lower 95.0%	Upper 95.0%
Intercept	- 2,448,259	1,618,973	- 1.5122	0.144708	- 5,805,803	909,284.2	- 5,805,803	909,284.2
Strain	4,839,139	373,999.2	12.9389	9.23E-12	4,063,512	5,614,766	4,063,512	5,614,766

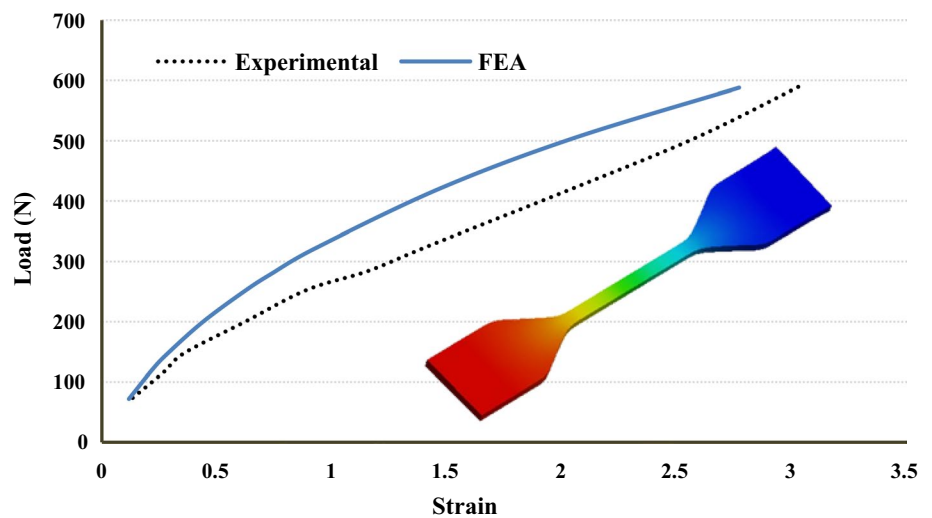
moduli and the characteristic time constants have been implemented in the model. The moduli are normalized according to the properties of the elastic component of the material including Density of 1200 kg/m³ and Young’s Modulus of 3.6 MPa. These data are summarized in Table 1.

To assess the impact of the rubber specifications on the overall behavior of the device, various rubber samples have been modeled and analyzed using the developed finite-element model using ANSYS Software version 2019 R1. The numerical results are then compared to the experimental data. The comparison between the data from the uniaxial

Table 3 Regression summary output for results of shear experimental test of the rubber

Regression statistics								
Multiple <i>R</i>	0.992552							
<i>R</i> square	0.985159							
Adjusted <i>R</i> square	0.98381							
Standard error	486,560.8							
Observations	13							
ANOVA								
	<i>df</i>	SS	MS	<i>F</i>	Significance <i>F</i>			
Regression	1	1.73E+14	1.73E+14	730.1947	2.08E−11			
Residual	11	2.6E+12	2.37E+11					
Total	12	1.75E+14						
	Coefficients	Standard error	<i>t</i> Stat	<i>p</i> value	Lower 95%	Upper 95%	Lower 95.0%	Upper 95.0%
Intercept	1,065,409	206,843.8	5.150789	0.000318	610,148.8	1,520,669	610,148.8	1,520,669
Strain	2,499,142	92,485.08	27.02212	2.08E-11	2,295,584	2,702,701	2,295,584	2,702,701

Fig. 6 Load–strain curve results for numerical analysis and experimental testing



experimental test and the results of the finite-element analysis demonstrates a promising agreement, as shown in Fig. 6.

4.1 Numerical model of rubber bracing damper

The finite-element model of the RBD device has been developed using ANSYS Software version 2019 R1 based on the previously validated data. The analysis of the RBD device takes into account large deflections, while the stress–strain curve is highly nonlinear but behaves elastically. The finite-element model of the RBD device, along with the mesh contours, is shown in Fig. 7.

Since the length of the rubber tube (*l*) which bonded to the inner and outer curved surfaces of the steel tubes (see Fig. 8) is long enough in comparison with its thickness,

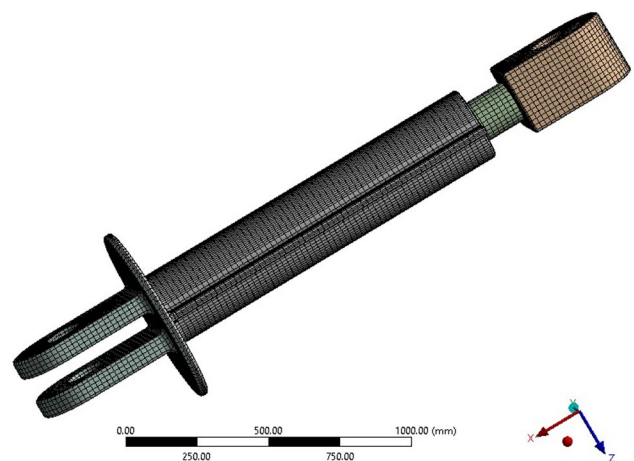


Fig. 7 RBD finite-element model

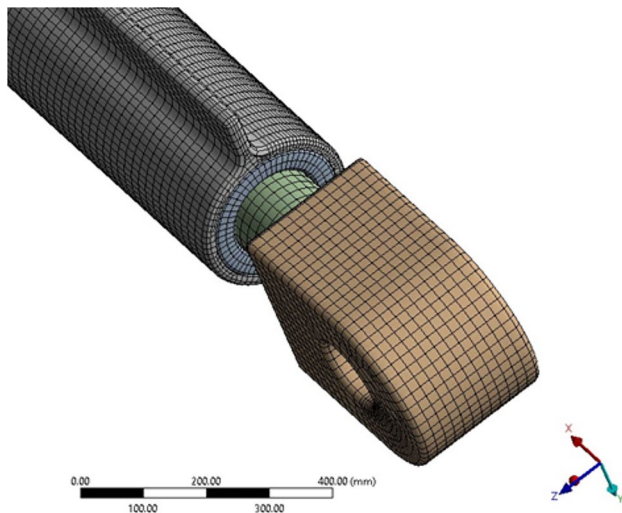


Fig. 8 Rubber tube bonded to the inner and outer curved steel surfaces

then the rubber material is assumed to be under simple shear stress.

In this case, axial stiffness is mainly calculated due to simple shear given by Eq. (3)

$$\frac{F}{d} = \frac{2\pi Gl}{\ln \frac{a_2}{a_1}}, \quad (3)$$

where d is the axial displacement, under axial force F . The shear modulus is G , and the inner and outer radius of the rubber tube is a_1 and a_2 . According to Eq. (3), the axial reaction force of the RBD device is dependent on the thickness, length, and shear modulus of the rubber material.

To investigate the relationship between the damping force and the rubber thickness, four different thicknesses of 10 mm, 20 mm, 30 mm, and 40 mm, all with a length of 1500 mm, were considered for implementation in the RBD device. These models were simulated under incremental loading at 100% elongation of the rubber material. Subsequently, an initial design for the RBD was proposed, and a finite-element model was developed. The dimensions and material properties used in the finite-element modeling of the RBD are summarized in Table 4.

The finite-element analysis was conducted by applying a displacement according to Fig. 9. The displacement was initially set at 2.5 mm in both pulling and pushing directions and was then increased to 5 mm, 7.5 mm, and 12.5 mm. The resultant damping forces of the RBD device increased up to 300 kN during these displacement steps.

Table 4 RBD device geometrical details and material properties

Length of the device	1600 mm
Diameter of the device	273 mm
Thickness of the outer cylinder	12.5 mm
Density of the steel	7850 kg/m ³
Young's modulus of the steel	2 e5 MPa
Shear modulus of the steel	7.7 e4 MPa
Length of the rubber layer	1500 mm
Diameter of the rubber layer	243 mm
Thickness of the rubber layer	42.5 mm
Density of the rubber layer	1200 kg/m ³
Young's modulus of the rubber layer	3.6 MPa
Shear modulus of the rubber layer	1.2 MPa

4.2 Finite-element analysis results for RBD

To investigate the nonlinear behavior of the viscoelastic material, a cyclic method was chosen for conducting the finite-element analysis. The total deflection of the inner core and rubber layer is illustrated in Fig. 10.

This deformation contour demonstrates that debonding of the rubber layer from the steel core occurs along with the movement of the steel core. However, the rubber layer attached to the outer steel tube shows no displacement during the operation of the device.

For a better understanding of the deflections of the rubber layer, a displacement contour at the joint of the front hinge and the inner core is shown in Fig. 11. It can be observed from this figure that the shear bulk modulus of the rubber resists the longitudinal displacement and works to dissipate vibrational energy.

Furthermore, to finalize the design parameters of the device, the equivalent Von-Mises stress and safety factor values in all segments of the RBD device, including the outer cylindrical tube, the inner core, and the rear hinge joint, are examined and presented in Fig. 12a–c, respectively.

The resulting data for these components indicate that the stress levels are within an appropriate range. Therefore, the damper device is capable of functioning with a reliable safety factor, and no damage or failure is predicted after applying dynamic loads to the device.

Finally, the hysteresis loop results (force–displacement graph) for the RBD device subjected to cyclic loads are shown in Fig. 13. In this graph, the area enclosed within the hysteresis loop represents the energy dissipated due to the shear action of the rubber (bulk modulus). As the imposed displacement increases, the resulting damping force and the

Fig. 9 Displacement pattern for the finite-element analysis

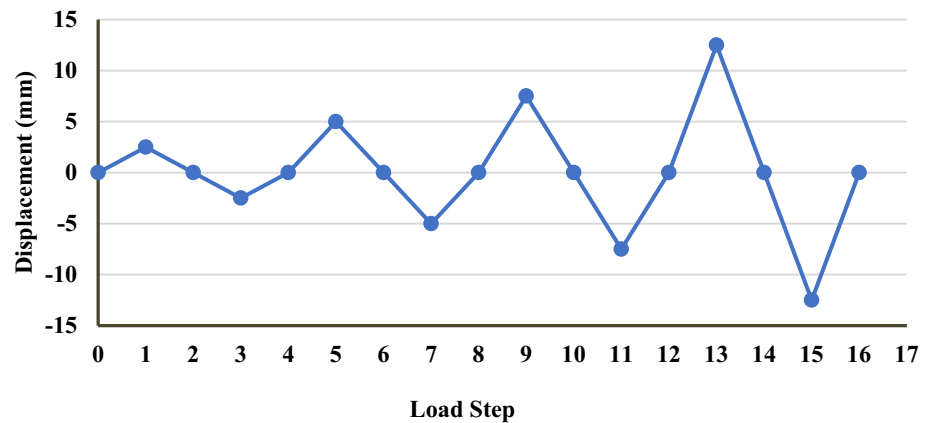


Fig. 10 Total deflection of under dynamic loads

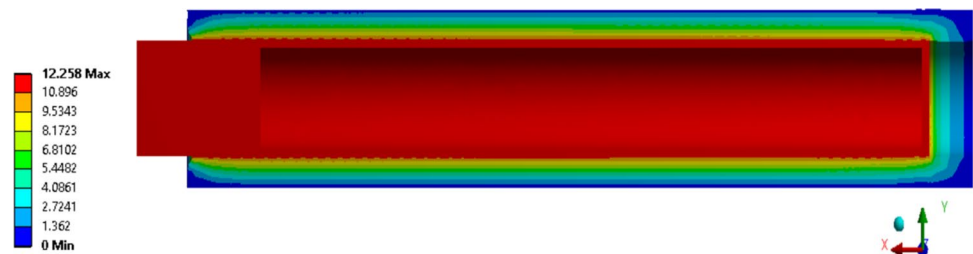
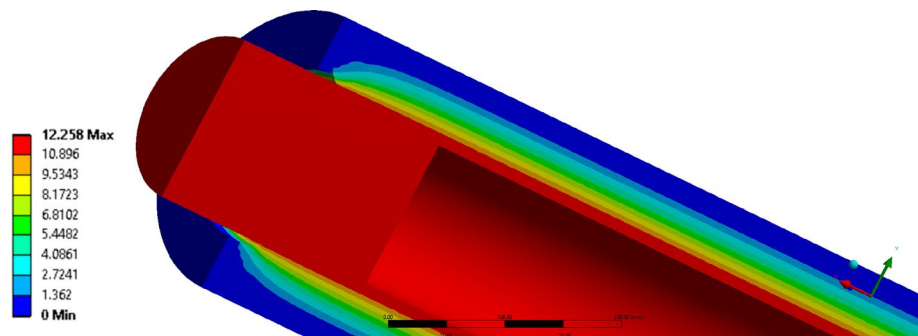


Fig. 11 Rubber deflection at the front hinge joint



amount of energy dissipation also increase. Since the incremental displacements applied to the device are small (due to the limited capacity of the actuator), the rubber does not exhibit nonlinear behavior, and the predicted force–displacement graph during loading closely resembles linear behavior. However, during unloading, the Prony Shear Relaxation effect of the rubber leads to nonlinear graphs.

In the first loading cycle, when a positive displacement of 2.5 mm is applied to the device, pushing the piston, the generated damping force increases to 54 kN. During unloading, the displacement and force return to zero. Continuing the loading procedure in the negative direction by pulling the piston, the finite-element model predicts identical results. For a – 2.5 mm displacement, a 54 kN force is generated. This cycle concludes with unloading the negative

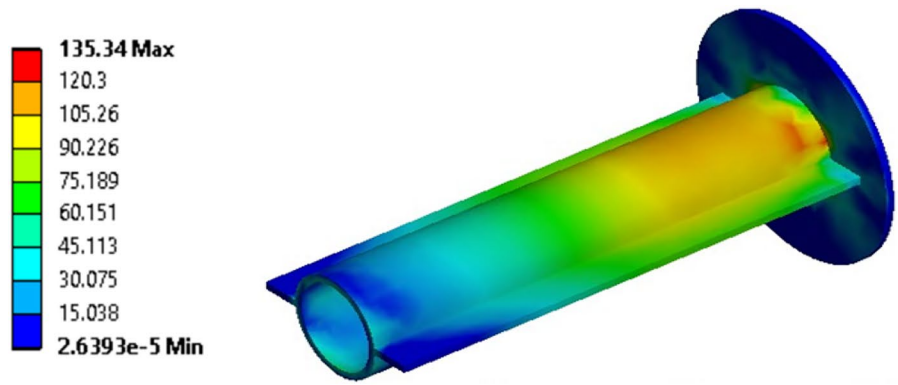
displacement, followed by the next cycle initiated by applying a 5 mm displacement to the device. This displacement is expected to generate a damping force of 113 kN, and for the 7.5 mm and 12 mm cyclic incremental displacements, the damping forces reach up to 173 kN and 280 kN, respectively.

Equivalent shear modulus G_{eq} and damping ratio H_{eq} have been defined by the use of Eq. (4) and Eq. (5), respectively. The equivalent stiffness K_{eq} obtained from Eq. (6) and the value of absorption energy W

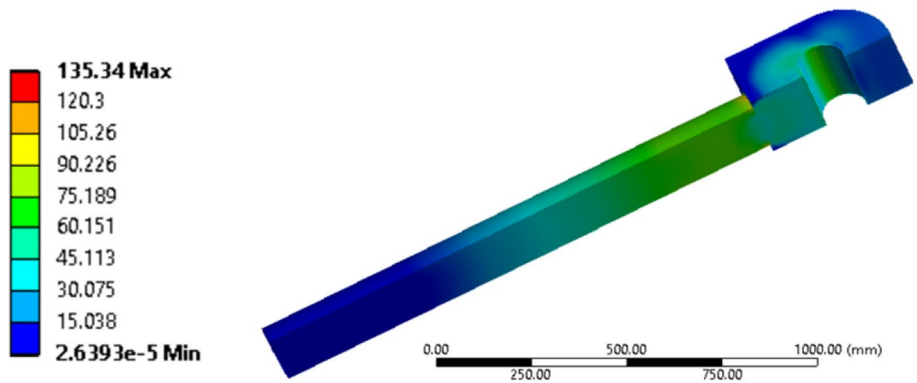
$$G_{eq} = \frac{K_{eq}}{(S/d)} [kN/mm^2], \quad (4)$$

where S is the sectional area of the viscoelastic part and d is its thickness

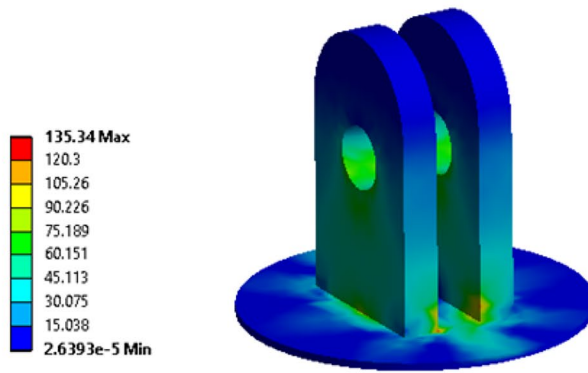
Fig. 12 Equivalent Von-Mises stress contour



(a) Stress distribution in the outer cylindrical tube



(b) Stress distribution in the inner core



(c) Stress distribution in rear hinge joint

$$H_{eq} = \frac{1}{4\pi} \cdot \frac{\Delta W}{W}, \tag{5}$$

where ΔW stands for absorption energy equal to the area of hysteresis loop and W denotes absorption energy

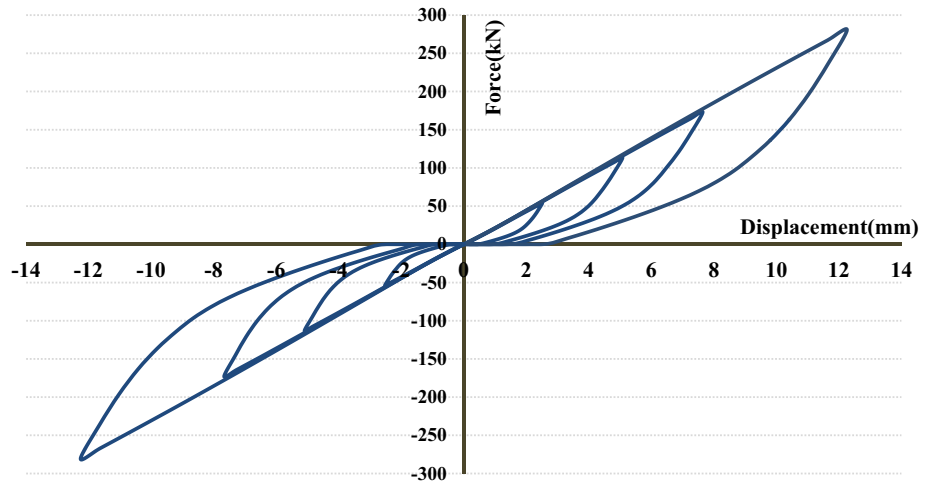
$$K_{eq} = \frac{P_{max} - P_{min}}{X_{max} - X_{min}} \text{ [kN/mm]}, \tag{6}$$

where $P_{max/min}$ shows maximum and minimum force and $X_{max/min}$ denotes the maximum and minimum displacement of the hysteresis loop.

The energy absorption is calculated using the following equation:

$$W = \frac{1}{2} \cdot X_{max} \cdot P_{max}, \tag{7}$$

Fig. 13 RBD device hysteresis loops predicted through developed finite-element model



where ω is dynamic test frequency.

The equivalent stiffness calculated from the numerical hysteresis loop is about 22.4 (kN/mm) with the damping ratio of 1135 (N·s/mm), and the amount of dissipated energy is equal to 1750 (kN.mm).

The prediction force for the rubber with 10mm thickness is obtained approximately as 200 kN using Eq. (3) at 100% elongation of the rubber. However, the FEM simulation results are showing 1500 kN force which is noticeable higher than results of imperial equation. Hence, by increasing rubber thickness from 10 till 40 mm, the results are much closer. As it can be seen in the graph, the resulting damping force for 40 mm thickness is obtained as 800 kN which is in good agreement with prediction.

In overall, the numerical results which presented in Fig. 14, when compared to the estimated force, demonstrate that the viscoelastic model of the rubber effectively operates under pure shear conditions up to 90% elongation. Hence, error for finite-element simulation becomes considerably pronounced in

lower rubber thickness. It may be due to the boundaries which considered in finite-element analysis for contact surface of the rubber with steel materials. Consequently, as mentioned earlier, the most accurate result has been obtained for the rubber with 42.5 mm thickness.

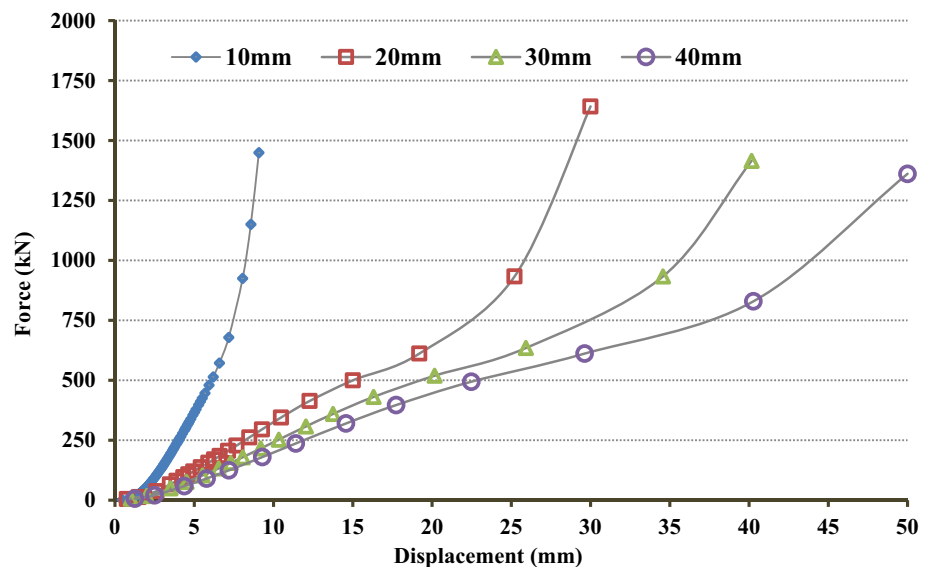
5 Development of analytical model for RBD

An attempt has been made to develop an analytical and finite-element model for the RBD device that is compatible with the frame element used to model other structural components such as beams and columns.

Considering L as the member length, and EI as the flexural rigidity, the stiffness components for the frame element may be calculated using Eq. (8) [18]

$$k_{rs} = \int_0^L EI(x)\Psi_r(x)\psi_s(x)dx. \tag{8}$$

Fig. 14 Force–displacement curves for RBD with different rubber thicknesses



By considering two hinges and rigid zones at both ends of frame element with length of dx and for hinge part and a and b for left and right rigid zones, respectively, the overall constitutive model for frame element can be depicted, as shown in Fig. 15, and the stiffness can be formulated by rewriting the above equation in the following form by adding rigid zones effect [6] as:

$$k_{rs} = \int_0^a EI\Psi_r(x)\Psi_s(x)dx + \int_0^c EI\Psi_r(x)\Psi_s(x)dx + \int_0^b EI\Psi_r(x)\Psi_s(x)dx. \tag{9}$$

Therefore, the constitutive model of the three-dimensional nonlinear RBD element has been derived base on the concept of introducing two separate zones in the model. These zones as showed in Fig. 16 consist of hinge zones (at both end of element) and damping zone.

Obviously, damping zone reflects the behavior of the damper and can be referred as an elastic/plastic element.

Hence, to derive the compatible constitutive model for RBD damper device, the axial stiffness component of RBD damper (K_D) is fitted within 12×12 size matrix in global coordinate as showed in Eq. (10), it can be deployed in the FEM program to use in 3D frame structures

$$KRBD = \begin{bmatrix} k_D & 0 & 0 & 0 & 0 & 0 & -k_D & 0 & 0 & 0 & 0 & 0 \\ 0 & 0 & 0 & 0 & 0 & 0 & 0 & 0 & 0 & 0 & 0 & 0 \\ 0 & 0 & 0 & 0 & 0 & 0 & 0 & 0 & 0 & 0 & 0 & 0 \\ 0 & 0 & 0 & 0 & 0 & 0 & 0 & 0 & 0 & 0 & 0 & 0 \\ 0 & 0 & 0 & 0 & 0 & 0 & 0 & 0 & 0 & 0 & 0 & 0 \\ 0 & 0 & 0 & 0 & 0 & 0 & 0 & 0 & 0 & 0 & 0 & 0 \\ 0 & 0 & 0 & 0 & 0 & 0 & 0 & 0 & 0 & 0 & 0 & 0 \\ -k_D & 0 & 0 & 0 & 0 & 0 & k_D & 0 & 0 & 0 & 0 & 0 \\ 0 & 0 & 0 & 0 & 0 & 0 & 0 & 0 & 0 & 0 & 0 & 0 \\ 0 & 0 & 0 & 0 & 0 & 0 & 0 & 0 & 0 & 0 & 0 & 0 \\ 0 & 0 & 0 & 0 & 0 & 0 & 0 & 0 & 0 & 0 & 0 & 0 \\ 0 & 0 & 0 & 0 & 0 & 0 & 0 & 0 & 0 & 0 & 0 & 0 \\ 0 & 0 & 0 & 0 & 0 & 0 & 0 & 0 & 0 & 0 & 0 & 0 \end{bmatrix}. \tag{10}$$

The same process was followed to derive the damping matrix for the RBD element.

Fig. 15 The constitutive model for frame element (beams and columns)

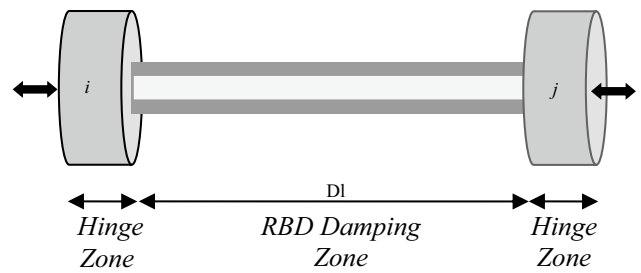
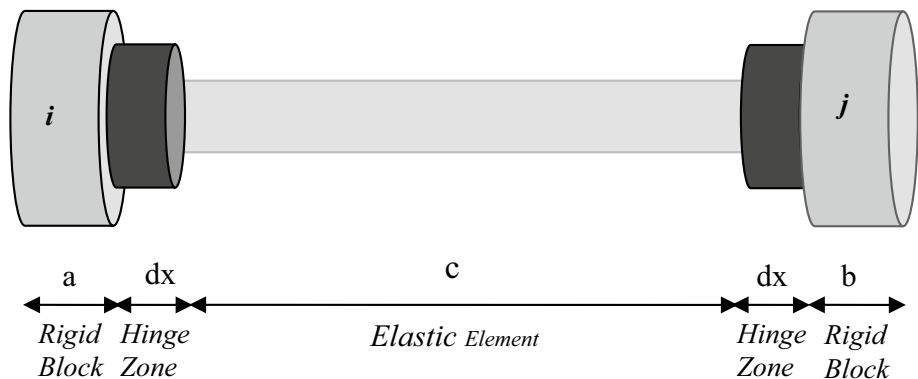


Fig. 16 Constitutive model for RBD

6 RBD prototype fabrication and test setup

The prototype of the RBD, shown in Fig. 17, has been fabricated, so that the rubber thickness in this device is considered as 42.5 mm and rubber is fully bonded to the inner surface of the steel cylinder tube and the outer surface of the inner rod. Table 5 demonstrates the dimensions of the fabricated prototype.

The prototype of the device and the test setup to the hard floor of the laboratory are illustrated in Fig. 18.

6.1 Incremental displacement test

To evaluate the performance of the developed RBD device, a horizontal dynamic actuator was used to apply a cyclic incremental displacement. The cyclic displacement was applied to the RBD device at different load speeds to assess the effect of applied load frequency on the damping force generated by the device. The resulting hysteresis loop from the experimental test is shown in Fig. 19. It reveals that the maximum displacement of 12 mm, applied at a frequency of 8 Hz to the RBD device, resulted in a peak resistance force of 300 kN.

Although the test was stopped at this stage due to the limited load capacity of the dynamic actuator, the equivalent stiffness computed from the extracted hysteresis loop is approximately 24 (kN/mm). The effective damping of



Figure 17 Fabrication of RBD prototype

Table 5 RBD prototype dimensions

Outer cylindrical tube (part 1)	Length (mm)	1600
	Diameter (mm)	273
	Thickness (mm)	30
Inner core (part 2)	Length (mm)	1800
	Diameter (mm)	158
	Thickness (mm)	20
Rubber tube (part 3)	Length (mm)	1500
	Diameter (mm)	243
	Thickness (mm)	42.5

the RBD device is measured to be 1244 (N·s/mm), and the amount of dissipated energy during the test is equal to 1875 (kN.mm).

Fig. 18 RBD experimental test setup



6.2 Cyclic load frequency test results

As mentioned earlier, the experimental test was repeated for excitation frequencies ranging from 1 to 8 Hz, and the performance of the RBD device was measured under different loading conditions. Figure 20 illustrates the hysteresis loops of the RBD device for various excitation frequencies. The results of the load–frequency test are summarized in Table 6. As predicted by numerical analysis, the damping force increases as the frequency of the applied load increases. This trend can be observed when the frequency is increased from 1 to 2 Hz, resulting in a load increase of approximately 5% from 232 to 247 kN. However, as reported in Table 6, during the experimental test, the dynamic actuator could not apply the same displacement to the device at 4 Hz and 8 Hz, preventing a direct comparison of the results.

6.3 Relaxation test results

A relaxation test was conducted on the RBD device, and the resistance force was observed, as shown in Fig. 21. When the RBD device was subjected to an initial constant displacement, only 25.7% of the applied displacement was released within the first minute of the relaxation test. During the relaxation time, the stress in the rubber decreased, indicating that the overall behavior of the device is dependent on the shear action of the rubber.

6.4 Numerical and experimental data validation

The finite-element simulation outcomes are compared with the test data, as shown in Fig. 22, demonstrating a very close agreement in terms of the force–displacement hysteresis curve. The characteristics of the RBD device, including effective damping, equivalent stiffness, and energy dissipation, obtained through numerical simulation by FEM and experimental tests, are tabulated in Table 7.

Fig. 19 Force–displacement result for RBD prototype test

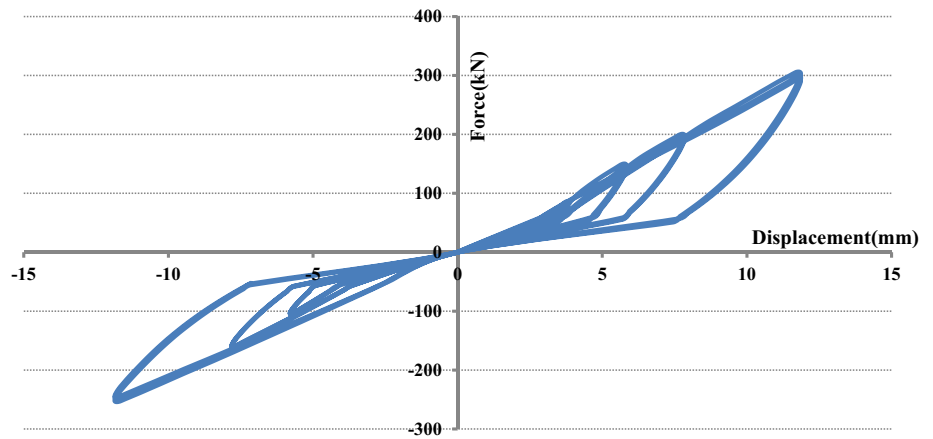


Fig. 20 RBD hysteresis loop under various excitation frequencies

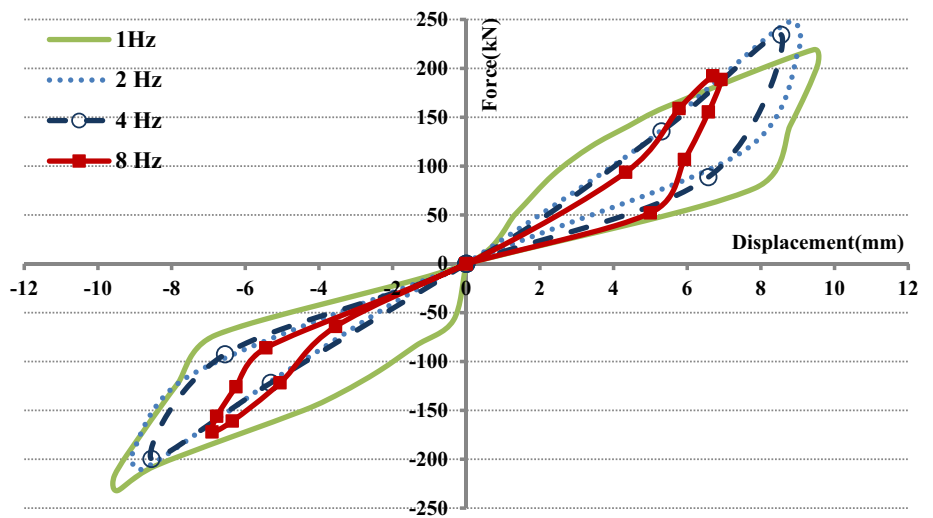


Table 6 Cyclic load frequency test results

Max displacement (mm)	Max damping load (kN)	Frequency (HZ)
6.9	172	8
8.5	200	4
8.8	247	2
9.5	232	1

The comparison between these two methods shows a difference of up to 8.76% for the finite-element numerical analysis, which is within an acceptable range. Therefore, the stiffness and damping coefficient extracted from the finite-element model have been used to develop a numerical model for the concrete frame structure equipped with the RBD device.

7 Implementing RBD devices in three-story building structure

7.1 Considered reinforced concrete frame structure

To examine the performance of the RBD device on a frame structure, a three-story reinforced concrete (RC) frame subjected to seismic excitation has been considered. This structure, as depicted in Fig. 23a, was experimentally investigated by Lu et al. [9] through shaking table tests and consists of two bays in the X-direction and one bay in the Z-direction. The details of the column and beam sections are presented in Fig. 23b, and the material properties are listed in Table 8. The steel bars have a concrete cover of 25mm. The three-story frame structure is subjected to the El Centro earthquake (USA-1940) record, and the response of the structure is investigated.

Fig. 21 RBD relaxation test result

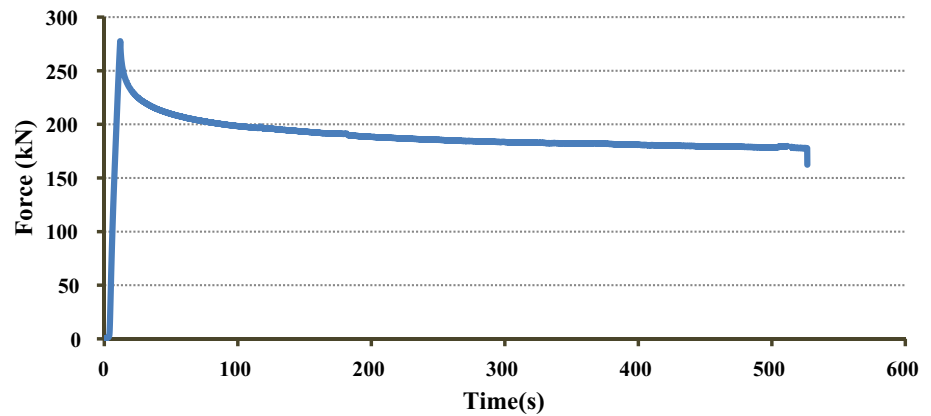


Fig. 22 Data validation

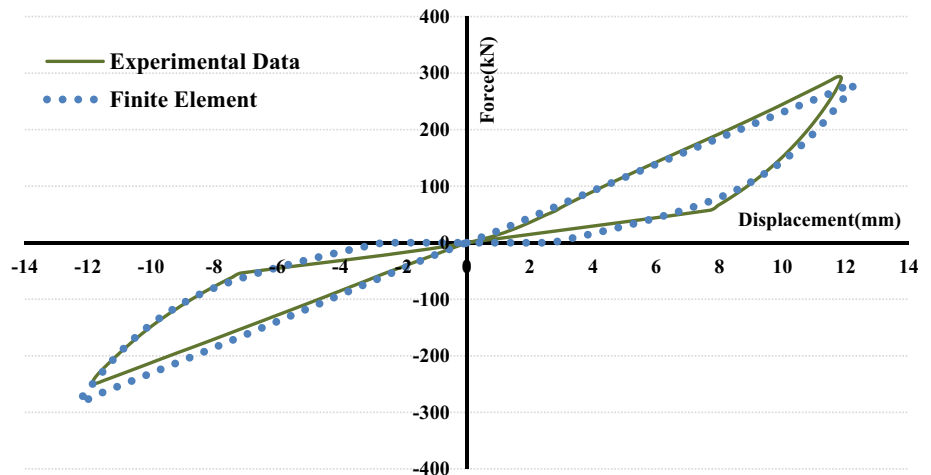


Table 7 Numerical and experimental results

RBD characteristics	Equivalent stiffness (kN/mm)	Damping ratio (N·s/mm)	Energy dissipation (kN·mm)
Experimental test	24	1244	1875
Numerical analysis	22.4	1135	1750
Error	6.67%	8.76%	6.67%

7.2 Implementing RBD device to finite-element program

To evaluate the dynamic behavior of reinforced concrete frames equipped with RBD devices, a specialized code named ARCS3D (Copyrighted, UPM 2015) has been developed and used to predict the pushover and time-history responses. This program has been coded using the Fortran language and is capable of simulating reinforced concrete (RC) structures furnished with damper devices. It can perform time-history dynamic analysis using the Newmark's algorithm with step-by-step integration method.

7.3 Verification of ARCS3D finite-element program

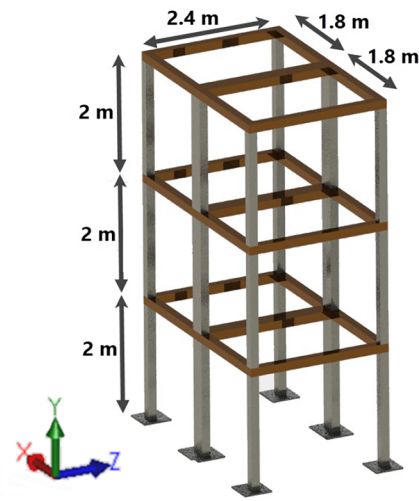
Before implementing the developed ARCS3D finite-element program, validation and verification of the program were conducted for the analysis of RC frames under earthquake excitations, and also RBD devices under cyclic loads. To this end, a three-story RC frame was examined, and the FEM results were cross-referenced with experimental testing outcomes found in the existing literature. Furthermore, the performance of the RBD device was validated against lab testing results, which were conducted as part of this study. Details of these validations are presented in the subsequent sections.

7.3.1 Validation of FEM model of frame in ARCS3D

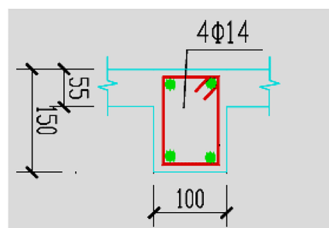
In this study, the developed finite-element program (ARCS3D) was verified by implementing it on a three-story RC frame that was tested by Lu et al. [9] under the El Centro (USA-1940) earthquake record. The FEM model of the three-story frame was developed, and a nonlinear time-history analysis was performed by applying the El Centro earthquake acceleration.



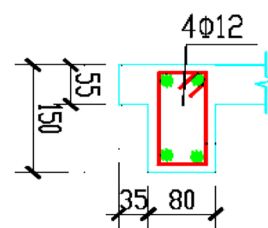
(a) former study (Lu et al, 2008)



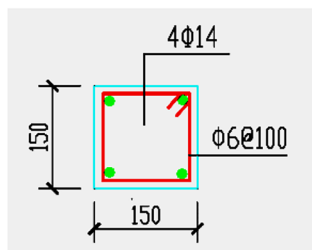
(b) Numerical model



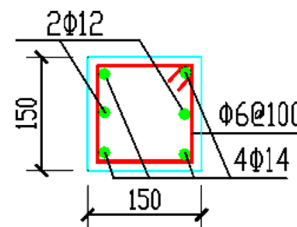
(i): Corner columns



(ii): Middle columns



(iii): Beam Sections



(iv): Beam section connected to the dampers

(c): Details for beams and columns

Fig. 23 Details of considered three-story RC frame structure

Table 8 Mechanical properties of three-story RC frame

Concrete compressive stress (N/mm ²)	20
Concrete modulus of elasticity (N/mm ²)	25,000
Steel yield stress (N/mm ²)	360
Steel ultimate stress (N/mm ²)	530
Steel modulus of elasticity (N/mm ²)	1.96 × 10 ⁵

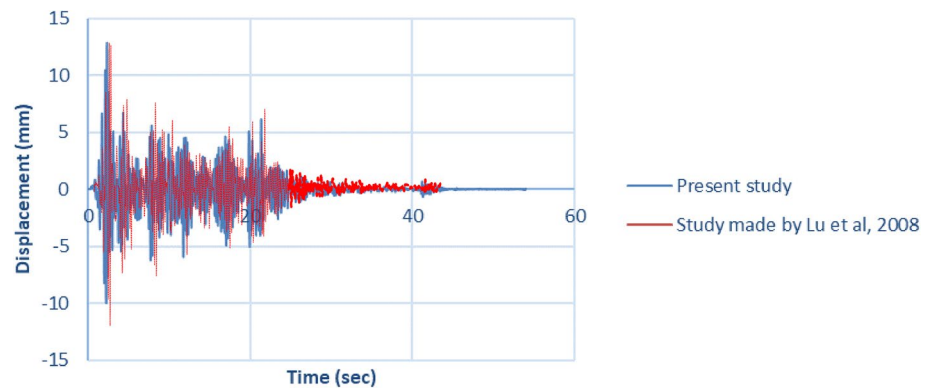
Figure 24 illustrates the comparison between the top-story displacement time-history obtained from the numerical analysis using the FEM program and the experimental

testing results conducted by Lu et al. [9]. The results show good agreement, indicating the accuracy of the numerical analysis in predicting the seismic response of the RC frame. The finite-element analysis error for the peak displacement of the top story is less than 6%, which is considered within an acceptable range.

7.3.2 Validation of FEM model of RBD in ARCS3D

In this study to validate the developed finite-element model for RBD device in ARCS3D, the results for experimental test of RBD have been used. For this purpose, the

Fig. 24 Time-history displacement of the top story



setup for experimental test has been considered in detail as shown in Fig. 25a to define the finite-element model according to the realistic conditions. Therefore, one end of RBD model is fixed by rigid support and the uniaxial force according to experimental test results has been applied to another end of RBD damper, as shown in Fig. 25b. Then nonlinear dynamic analysis has been conducted and displacement results have been compared with the experimental test. The comparison between force–displacement results for experimental test which has been considered in

here as benchmark and also results of analysis by ARCS3D for RBD device has been presented in Fig. 26.

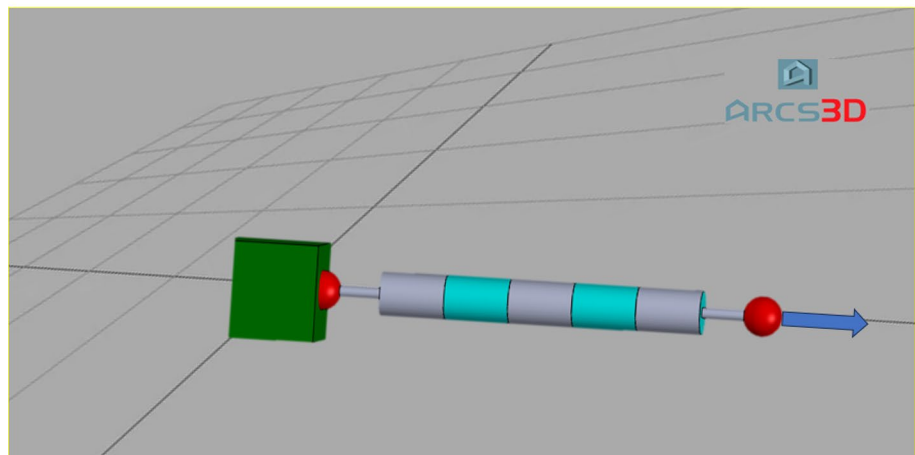
As it can be seen in this figure, the results are in very good agreement and maximum error which has been calculated as 7.7% which is due to roundoff for stress–strain regression equation and also considering fully rigid support in ARCS3D finite-element program. Although in experimental testing, there was some sliding in the support and bolts and nuts of connections.

Therefore, the finite-element model of RBD has been validated via experimental test results with a good accuracy.

Fig. 25 Validation of finite-element modeling of RBD in ARCS3D through experimental test results



(a) Experimental test setup for RBD device



(b) RBD finite element model in ARCS3D according to experimental test setup

7.4 Implementing RBD device to finite-element program

The constitutive model for RBD device has been developed using the results of the experimental test which explained before, to extract the damper characteristics to use in finite-element simulation by ARCS3D program.

For this purpose, the stiffness of the device was calculated for each incremental displacement, and a stiffness–displacement curve was obtained, as shown in Fig. 27. Based on this curve, a polynomial equation was formulated to represent the nonlinear relationship between stiffness and displacement. This equation was then used to calculate the RBD stiffness corresponding to the applied displacement, as presented here

$$K_{RBD} = \beta_1 + \beta_2 \times \delta + \beta_3 \times \delta^2 + \beta_4 \times \delta^3 + \beta_5 \times \delta^4 + \beta_6 \times \delta^5, \tag{11}$$

where β is damper parameter and δ stands for incremental displacement. Calculated β values are shown in Table 9.

Also, the device effective damping is calculated as 1244 (N·s/mm) using hysteresis graph which obtained through conducting experimental test.

7.5 Parametric study

In this study, a parametric study was conducted to evaluate the effect of the damping coefficient on the seismic response of the structure. In addition to the calculated damping coefficient (1244 N·S/mm) for the tested RBD device in this

Fig. 26 Comparison of ARCS3D analysis results for RBD with experimental testing results

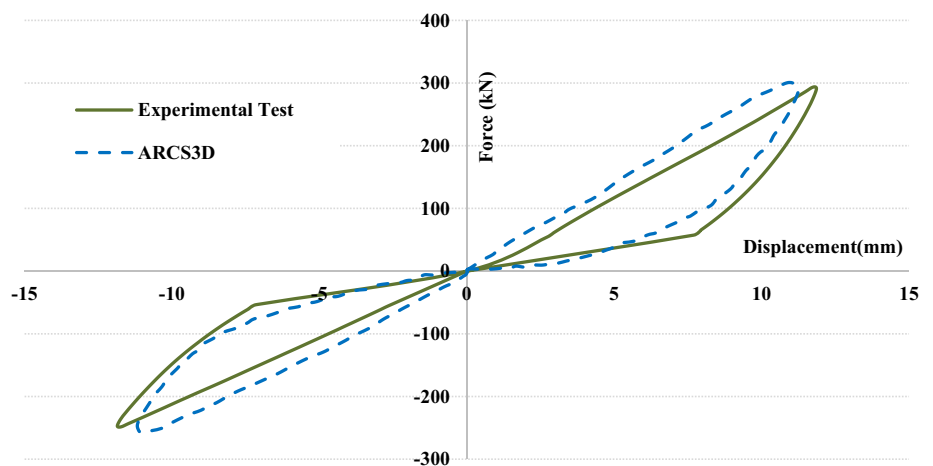


Fig. 27 RBD stiffness versus displacement diagram

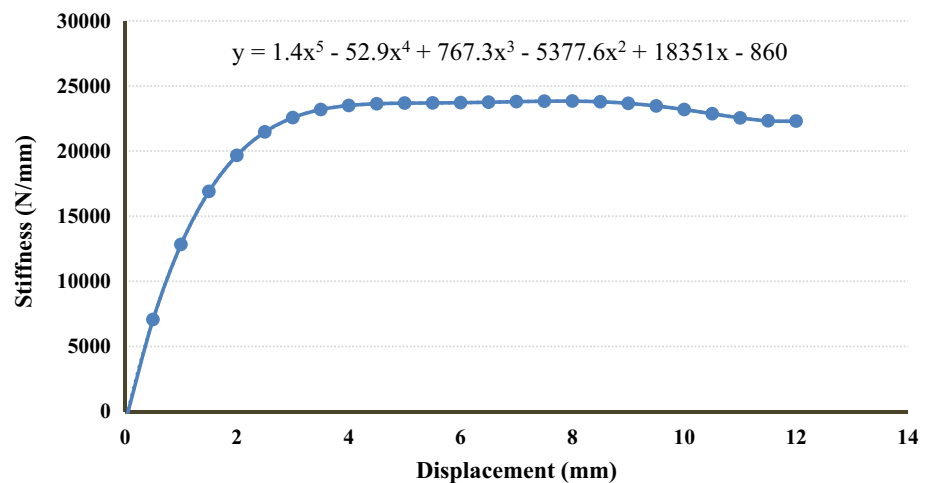


Table 9 RBD parameters

β_1	β_2	β_3	β_4	β_5	β_6	Displacement limit [mm]	Initial effective stiffness [N/mm]
- 860.0	18,351	- 5377.6	767.3	- 52.9	1.4	20	17,500

Table 10 Damping coefficients applied for parametric study

Label	RBD1	RBD2	RBD3	RBD4	RBD5
Damping coefficient (N·S/mm)	1244	5000	10,000	15,000	20,000

study, four additional damping coefficients (5000, 10,000, 15,000, and 20,000 N·S/mm) corresponding to upscaled RBD devices were considered, as listed in Table 10.

It is worthy to mention that damping coefficient is related to two factors of damping characteristics of the rubber (material properties) and also area under force–displacement curve (hysteresis loop). Therefore, to scale up the proposed damper for higher damping performance, it is required to employ rubber with higher damping characteristics and also increase the size of device (geometry parameters) to increase resistant damping force and corresponding displacement to have higher damping coefficient.

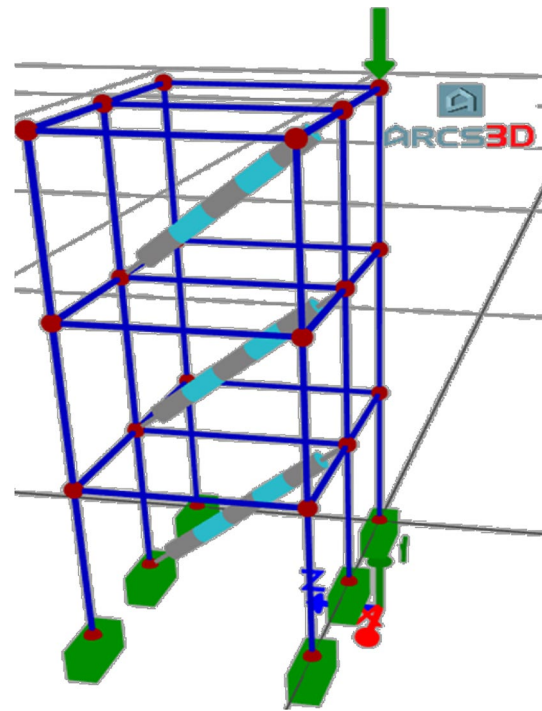
The input file was prepared to define the initial configuration of the three-story RC frame equipped with the RBD device in the middle frame, as depicted in Fig. 28. All material properties and loading details were coded using MATLAB program, which was linked with the ARCS3D finite element program to conduct time-history nonlinear analysis of the structure with different damping coefficients under El Centro earthquake excitation. During this process, the nodal displacements, structural member forces, and plastic hinges were recorded for the structures with RBD1–RBD5 to investigate the effect of the rubber damping parameter on the seismic response of the structure.

7.6 Results and discussion

As mentioned before, the time-history analysis was conducted to investigate the seismic response of the considered three-story frame equipped with five different RBD devices (RBD1 to RBD5). The time-history displacement of the bare frame (at the top floor) and the frames equipped with different RBD devices, subjected to the El Centro earthquake record (USA-1940), are shown in Figs. 29.

As seen in the figure, the comparison of the displacement response between the structure equipped with RBD devices and the bare frame demonstrates that implementing RBD dampers effectively reduces the movement of the structure. Moreover, these results indicate that structures furnished with RBD devices with higher damping coefficients exhibit greater displacement reduction. As expected, higher damping devices result in more energy dissipation and lower structural movement.

This discussion can be further supported by examining the maximum and minimum displacements, as presented in Table 11. The results show a reduction of 20.8%, 41.39%,

**Fig. 28** Initial configurations of the structure

53.79%, 61.72%, and 66.97% for maximum displacement, and reductions of 0.9%, 5.45%, 17.07%, 29.162%, and 40.01% for minimum displacement, for the frame equipped with RBD (1), RBD (2), RBD (3), RBD (4), and RBD (5), respectively, compared to the response of the bare frame. Consequently, a significant reduction in structural movement is observed with increasing damping coefficient, as expected.

To evaluate the effect of using RBD damper devices on structural member forces, the internal forces in the columns of the structure equipped with RBD dampers are compared to those of the bare frame. Table 12 presents the axial forces, shear forces, and bending moments that develop in the first-story columns in the middle of the frame under El Centro earthquake loading. The notations “2–2” and “3–3” designate the member forces in the X- and Z-directions, respectively (refer to Fig. 23 for direction designations).

The maximum axial force increases from 1.92 kN in the bare structure to 3.25 kN in the structure equipped with RBD1. Furthermore, the axial force increases to 5.2 kN, 7.2 kN, 8.2 kN, and 9.2 kN for the frames with RBD (2), RBD (3), RBD (4), and RBD (5), respectively. This increase is attributed to the action of the RBD devices in generating damping forces to dissipate the structural movement, which causes a transfer of some of the damper force to the structural column connected to the damper through the joints. Therefore, RBD devices with higher damping coefficients, such as RBD (5), generate greater resistant forces, resulting

Fig. 29 Time-history of the upper floor displacement

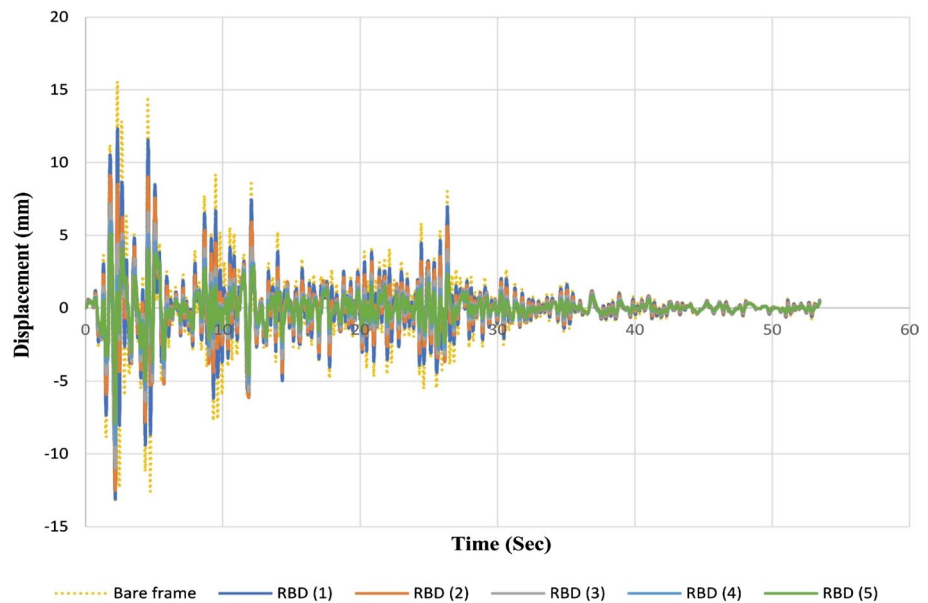


Table 11 Comparative maximum displacement in the horizontal direction for each structure case under El Centro earthquake accelerations

Structure type	MAX displacement (mm)	MIN displacement (mm)
Bare frame	15.56	- 13.24
RBD (1)	12.33	- 13.12
RBD (2)	9.12	- 12.52
RBD (3)	7.19	- 10.98
RBD (4)	5.96	- 9.38
RBD (5)	5.14	- 7.94
Reduction percentage for RBD (1)	20.8%	0.9%
Reduction percentage for RBD (2)	41.39%	5.45%
Reduction percentage for RBD (3)	53.79%	17.07%
Reduction percentage for RBD (4)	61.72%	29.162%
Reduction percentage for RBD (5)	66.97%	40.01%

in higher forces being transmitted to the columns, despite the greater displacement reduction.

Similarly, the shear force and moment in the direction of the applied seismic excitation increase in the middle column of the frame furnished with RBD devices compared to the bare frame, due to the effect of RBD damper force during its operation. However, unlike the axial force, the shear and moment decrease in frames when RBD devices with higher damping coefficients are employed. This occurs, because, as mentioned before, the function of the RBD damper device is primarily in the axial direction, resulting in an increase in the axial force of the column. However, since the overall movement of the structure is reduced, the shear and moment in the column of the frame with a higher damping coefficient for RBD devices are reduced.

The internal forces in the corner column, for both the bare frame and the frame equipped with RBD devices, are

Table 12 Maximum forces and moments in the RBD braced column and unbraced

Structure type	Bare frame	RBD (1)	RBD (2)	RBD (3)	RBD (4)	RBD (5)
MAX axial force (N)	1920.7	3246.5	5228.7	7600.2	8710.9	9258
MIN axial force (N)	- 2093.4	- 2839.8	- 3591	- 4010	- 4572.2	- 4828.7
MAX shear force (N) 2-2	830.94	1616.4	1546.1	1374.4	1207.2	1067.7
MIN shear force (N) 2-2	- 782.95	- 1332.1	- 1109.3	- 895.62	- 758.6	- 673.16
MAX shear force (N) 3-3	619.48	619.71	620.04	620.95	621.71	623.41
MIN shear force (N) 3-3	- 490.94	- 490.84	- 490.76	- 491.23	- 490.02	- 490.76
MAX moment (N.m) 2-2	1.27E+06	2.58E+06	2.05E+06	1.64E+06	1.38E+06	1.21E+06
MIN moment (N.m) 2-2	- 1.41E+06	- 2.98E+06	- 2.84E+06	- 2.50E+06	- 2.19E+06	- 1.90E+06
MAX moment (N.m) 3-3	2.35E+06	2.35E+06	2.35E+06	2.35E+06	2.35E+06	2.35E+06
MIN moment (N.m) 3-3	- 2.01E+06	- 2.01E+06	- 2.01E+06	- 2.01E+06	- 2.01E+06	- 2.01E+06

Table 13 Maximum forces and moments in the corner column in the RBD braced structure and unbraced

Structure type	Bare frame	RBD (1)	RBD (2)	RBD (3)	RBD (4)	RBD (5)
MAX force (N)	3819.7	4332.1	3766.3	3177.8	3238.1	3409.3
MIN force (N)	- 3727.6	- 5250.6	- 4846.9	- 4487.8	- 4396.6	- 4276.7
MAX shear force (N) 2–2	927.95	1883.2	1800.4	1597.6	1402.6	1237.8
MIN shear force (N) 2–2	- 860.2	- 1585.9	- 1296.2	- 1049.6	- 885.74	- 781.29
MAX shear force (N) 3–3	9023.3	8918.7	10,819	14,147	20,270	23,033
MIN shear force (N) 3–3	- 7913.8	- 6142.8	- 7947.8	- 10,653	- 12,274	- 13,213
MAX moment (N.m) 2–2	1.30E+06	2.76E+06	2.17E+06	1.74E+06	1.47E+06	1.28E+06
MIN moment (N.m) 2–2	- 1.47E+06	- 3.16E+06	- 3.02E+06	- 2.66E+06	- 2.32E+06	- 2.02E+06
MAX moment (N.m) 3–3	2.09E+06	2.09E+06	2.09E+06	2.09E+06	2.09E+06	2.09E+06
MIN moment (N.m) 3–3	- 1.78E+06	- 1.78E+06	- 1.78E+06	- 1.78E+06	- 1.78E+06	- 1.78E+06

presented in Table 13. From these results, it can be observed that the internal force of the corner column is higher when the frame is furnished with RBD devices compared to the bare frame, due to the damping force generated by the RBD devices. Similarly, the internal axial forces increase when RBD devices with higher damping coefficients are used, indicating the effect of the damping coefficient in generating higher damper forces. However, the shear and moment decrease when RBD devices with higher damping coefficients are utilized.

By comparing the forces in the middle column and the corner column, it is evident that the corner column experiences higher forces due to the overall structural moment during the movement of the structure under earthquake excitation.

Hence, the implementation of RBD damper devices increases the damping capacity of the structure and shows promise in improving the structural responses by reducing the displacement of the frame. However, the analysis results indicate that despite the increase in axial forces of the columns due to the damping force, there were no plastic hinges or yielding observed in any of the structural members under the applied El Centro earthquake record, and all beams and columns exhibited sufficient strength to withstand the transferred forces.

8 Conclusion

In the current study, a new Rubber Bracing Damper (RBD) was developed based on the viscoelastic behavior of high damping natural rubber material. This device is suitable for structures exposed to extreme dynamic loads for the purpose of energy dissipation.

The material model for the rubber utilized in this study was based on the Neo-Hookean theory combined with the viscoelastic shear and Prony Shear Relaxation method, derived from experimental test results. The finite-element

analysis results demonstrate that the proposed RBD device exhibits promising performance when subjected to incremental displacements. The thickness of the rubber was found to have a significant effect on the resulting damping force. Varying the rubber thickness of the RBD device from 10 to 40 mm resulted in a change in generated force from 200 to 800 kN for 100% elongation of the rubber.

Subsequently, experimental tests were conducted on a lab-size prototype using a dynamic actuator. The excellent agreement between the finite-element data and experimental results confirms the efficiency of the developed RBD device in dissipating vibration energy and generating damping force.

For the dynamic analysis of a frame structure equipped with RBD devices, a constitutive model for the damper was derived and implemented in the finite-element code. A comprehensive parametric study was also conducted to investigate the effect of the damping parameters of the RBD on the seismic response of the frame structure.

The results demonstrate that the displacement of the structures equipped with RBD devices can be reduced by up to 66.97%. Furthermore, the axial force in the main columns increases due to the function of the RBD damper device in generating damping force, while the shear and moment in the considered columns are decreased. Importantly, no plastic hinges were observed in the structural members of the frame under the applied seismic excitation. Therefore, it can be concluded that the RBD device is successful in protecting the structure against severe vibrations and dissipating structural movement.

Declarations

Conflict of interest It is declared that there is no conflict of interest in this research work.

Compliance with ethical standards There is no ethical concern in this research work.

Open Access This article is licensed under a Creative Commons Attribution 4.0 International License, which permits use, sharing, adaptation, distribution and reproduction in any medium or format, as long as you give appropriate credit to the original author(s) and the source, provide a link to the Creative Commons licence, and indicate if changes were made. The images or other third party material in this article are included in the article's Creative Commons licence, unless indicated otherwise in a credit line to the material. If material is not included in the article's Creative Commons licence and your intended use is not permitted by statutory regulation or exceeds the permitted use, you will need to obtain permission directly from the copyright holder. To view a copy of this licence, visit <http://creativecommons.org/licenses/by/4.0/>.

References

- Bartera F, Dezi L, Giacchetti R. Cyclic behaviour of a reinforced concrete braced frame with high damping rubber devices. *WIT Trans Built Environ*. 2004. <https://doi.org/10.2495/SU040411>.
- Fang X, Zhou Y, Bi K, Hao H, Wang T. Experimental study on the cyclic behaviors of an innovative lead-viscoelastic coupling beam damper (LVCBD). *J Build Eng*. 2023;64:105596.
- Farahpour H, Hejazi F. Development of integrated semi-active adaptive vibration control system for bridges subjected to traffic loads. *Structures*. 2023;51:1773–94.
- Gauron O, Girard O, Paultre P, Proulx J. Design and performance of autonomous chevron-brace systems with elastomeric-dampers for steel frames. *J Constr Steel Res*. 2015;115:34–46.
- Hristov JY. Linear viscoelastic responses: The Prony decomposition naturally leads into the Caputo-Fabrizio fractional operator. *Front Phys*. 2018;6:135.
- Hejazi F, Farahpour H, Ayyash N, Chong T. Development of a volumetric compression restrainer for structures subjected to vibration. *J Build Eng*. 2022;46:103735.
- Ishikawa S, Tanaka K, Yano D, Kijimoto S. Design of a disc-shaped viscoelastic damping material attached to a cylindrical pipe as a dynamic absorber or Houde dampe. *J Sound Vib*. 2020;475:115272.
- Li HN, Fu X, Li YL, Liu HJ. Mechanical model and structural control performance of a new rotation-magnified viscoelastic damper. *Eng Struct*. 2022;252:113569.
- Lu X, Zhou Y, Yan F. Shaking table test and numerical analysis of RC frames with viscous wall dampers. *J Struct Eng*. 2008;134(1):64–76.
- Modhej A, Zahrai SM. Numerical study of visco-hyperelastic damper with high axial damping rubber subjected to harmonic loading. *Structures*. 2021;29:1550–61.
- Ismail M. An elastoplastic bracing system for structural vibration control. *Eng Struct*. 2019;200(1): 109671.
- Ramakrishna U, Mohan SC. Performance of low-cost viscoelastic damper for coupling adjacent structures subjected dynamic loads. *Mater Today: Proc*. 2019;28:1024–9.
- Ranaei O, Aghakouchak AA. A new hybrid energy dissipation system with viscoelastic and flexural yielding strips dampers for multi-level vibration control. *Arch Civ Mech Eng*. 2019;19(2):584–97.
- Rahnavard R, Rebelo C, Craveiro HD, Napolitano R. Numerical investigation of the cyclic performance of reinforced concrete frames equipped with a combination of a rubber core and a U-shaped metallic damper. *Eng Struct*. 2020;225: 111307.
- Sheikhi J, Fathi M, Rahnavard R, Napolitano R. Numerical analysis of natural rubber bearing equipped with steel and shape memory alloys dampers. *Structures*. 2021;32:1839–55.
- Shu Z, Li G, Xu Q, Leng Y. Rotational viscoelastic dampers for steel buckling-restrained braced frames: concept, validation, and evaluation. *J Build Eng*. 2023;74: 106597 (**Available online 11 May 2023**).
- Soltanabadi R, Mamazizi A, Behnamfar F. Evaluating the performance of chevron braced frame with RSCD viscoplastic damper. *Eng Struct*. 2020;206: 110190.
- Thanoon WA, Paul DK, Jaafar MS, Trikha DN. Influence of torsion on the inelastic response of three-dimensional R. C frames. 2004;40:611–28.
- Uang CM, Bertero VV. Evaluation of seismic energy in structures. *Earthq Eng Struct Dyn*. 1990;19(1):77–90.
- Xiang Y, Xie HR. Probabilistic effectiveness of visco-elastic dampers considering earthquake excitation uncertainty and ambient temperature fluctuation. *Eng Struct*. 2021;226: 111379.
- Xu ZD, Yang Y, Zhu YN, Ge T. Experimental study and mathematical modeling of viscoelastic dampers with wider temperature range based on blended rubber matrix. *J Build Eng*. 2023;70(1): 106414.
- Zhang S, Hou H, Qu B, Zhu Y, Li K, Fu X. Tests of a novel re-centering damper with SMA rods and friction wedges. *Eng Struct*. 2021;236: 112125.
- Zhou L, Alam MS, Song A, Ye A. Probability-based residual displacement estimation of unbonded laminated rubber bearing supported highway bridges retrofitted with Transverse Steel Damper. *Eng Struct*. 2022;272: 115053.
- Zienkiewicz OC, Taylor RL, Fox D. The finite element method for solid and structural mechanics. 7th ed. Elsevier; 2014. <https://doi.org/10.1016/B978-1-85617-634-7.00004-1>.
- Zeynali K, Monir HS, Mirzai NM, Hu JW. Experimental and numerical investigation of lead-rubber dampers in chevron concentrically braced frames. *Arch Civ Mech Eng*. 2018;18:162–78.

Publisher's Note Springer Nature remains neutral with regard to jurisdictional claims in published maps and institutional affiliations.